RSC Advances

PAPER

View Article Online
View Journal | View Issue

Cite this: *RSC Adv.*, 2020, **10**, 38416

Semiconductor ZnO based photosensitizer core–shell upconversion nanoparticle heterojunction for photodynamic therapy

Yongmei Li, *[a] Yuemei Li, [b] Yandong Bai,[c] Rui Wang, [d] Laixiang Lin[a] and Yina Sun[a]

Photodynamic therapy (PDT) as a noninvasive technique is widely used to treat cancer diseases due to its low side effects. PDT based on upconversion nanoparticles (UCNPs) improved tissue penetration and photo-stability. However, traditional photosensitizers and UCNPs were difficult to incorporate, which limited the circulation of the UCNPs in blood and decreased the PDT effect. Herein, we designed $NaErF_4$@ZnO UCNPs for potential application in thyroid tumor cell PDT. With ZnO coated on $NaErF_4$, the blue (415 nm), green (525 nm/545 nm) and red (661 nm) upconversion luminescence enhanced compared with that of $NaErF_4$ core nanoparticles. Particularly, the generation of UV upconversion emission by $NaErF_4$ sensitized ZnO, which catalyzed H_2O and O_2 to produce ROS reactive oxygen species (ROS) to induce papillary thyroid carcinoma (PTC) cell lines BHP 5-16. With 1000 μg mL^{-1} of $NaErF_4$@ZnO UCNPs, the viability of BHP 5-16 cells decreased to about 41% as measured by CCK8 assay with 980 nm NIR irradiation. Moreover, it was confirmed that $NaErF_4$@ZnO UCNPs had low toxicity for BHP 5-16 cells. All these results indicated that $NaErF_4$@ZnO upconversion nanoparticles were an excellent platform for PDT treatment.

Received 31st August 2020
Accepted 12th October 2020

DOI: 10.1039/d0ra07466g

rsc.li/rsc-advances

Introduction

Photodynamic therapy (PDT) is a noninvasive treatment technique, which utilizes photosensitizers to produce reactive oxygen species (ROS).[1–3] ROS include hydroxyl radicals (˙OH), singlet oxygen ($^1O_2$) and hydrogen peroxide (H_2O_2), which can cause oxidative damage to cells.[4–6] Compared with normal cells, the ROS levels had an important influence on cancer cells. The PDT technique can treat cancer and other malignant diseases.[7–16] However, the further development of PDT was limited to photosensitizers. Most of the photosensitizers were sensitized by ultraviolet (UV) and visible (vis) light, which decreased tissue penetration of the PDT treatment.[17–19]

Rare earth-doped upconversion nanoparticles (UCNPs) had attracted great interest recently owing to their unique photophysical capabilities.[20–22] Upconversion luminescence (UCL) was anti-Stokes optical process, which can convert near infrared (NIR) light into UV and vis light.[23–27] The wavelength of NIR light ranged from 700 nm to 1500 nm, which located in biological spectroscopy window.[28–30] Therefore, UCNPs had great potential application in PDT treatment due to their high tissue penetration, low fluorescence background, good photo-stability and high signal-to-noise ratio.[31,32] However, the tradition PDT treatment based on UCNPs needed to combine photosensitizers. The photosensitizers loaded on as-synthesized UCNPs, which limited to the circulation of the UCNPs in blood and decreased the PDT effect.[33,34] In addition, most of photosensitizers were organic compound and purchases, increasing the PDT treatment costs and toxicity.

Zinc oxide (ZnO) provided a new way to improve this problem owing to its high chemical stability, high thermal stability and low toxicity.[35–37] ZnO nanoparticle as a semiconductor had wide band gap about 3.37 eV, which matched with emission peaks range from 330 nm to 400 nm, and UCNPs can radiated this wavelength of UV.[38,39] ZnO nanoparticle was a promising photosensitizer, which can be easily embedded into UCNPs.

In this work, we synthesized $NaErF_4$@ZnO UCNPs for PDT application. $NaErF_4$ excited UV upconversion luminescence and sensitized the ZnO to generate the ROS. After ZnO coated on $NaErF_4$, the intensities of upconversion emission enhanced compared with that of $NaErF_4$ nanoparticles. ROS of $NaErF_4$@ZnO UCNPs produced with 980 nm NIR light irradiation, and the NIR irradiation increased the deep of tissue

[a]*NHC Key Laboratory of Hormones and Development, Tianjin Key Laboratory of Metabolic Diseases, Chu Hsien-I Memorial Hospital & Tianjin Institute of Endocrinology, Tianjin Medical University, No. 6 Huanrui North Road, Ruijing Street, Beichen District, Tianjin, 300134, China. E-mail: liyongmei0811@sina.com*
[b]*Xiamen Cardiovascular Hospital, Xiamen University, No. 2999 Jinshan Road, Huli District, Xiamen, Fujian 361015, China*
[c]*Tianjin Union Medical Center, No. 190 Jieyuan Road, Hongqiao District, Tianjin, 300121, China*
[d]*School of Chemistry and Chemical Engineering, Harbin Institute of Technology, No. 92 Xi Dazhi Street, Nangang District, Harbin, Heilongjiang 150001, China*

penetration. The evaluation of cell viability based on CCK8 assay method had an outstanding effect on photodynamic therapy for thyroid tumor cells. In addition, the $NaErF_4$@ZnO UCNPs had low toxicity for BHP 5-16 cells. These results indicated that as-prepared $NaErF_4$@ZnO UCNPs were excellent platform for PDT treatment.

Result and discussion

Fig. 1 illustrated 980 nm NIR laser-activated, mitochondria-targeted upconversion $NaErF_4$@ZnO nanoparticles for amplified photodynamic therapy (PDT). We designed ZnO coated $NaErF_4$ upconversion nanoparticles. $NaErF_4$ can be excited the UV and visible upconversion emission *via* the excitation at 980 nm NIR light. These UV and visible light from $NaErF_4$ can be used by ZnO. The upconverted UV light triggered the photogenerated electrons in the valence band of the ZnO to the conduction band, thus resulting in the formation of photoinduced electron–hole (e^-–h^+) pair, which catalyzed H_2O and O_2 produce ROS and induced cancer cell apoptosis. The NIR excitation light (980 nm) had high tissue penetration, which leaded to amplified therapeutic efficacy.

Fig. 2 performed X-ray diffraction patterns (XRD) of the as-synthesized $NaErF_4$ coating ZnO ($NaErF_4$@ZnO) upconversion nanoparticles. The XRD diffraction peaks of $NaErF_4$@ZnO can be assigned to two crystalline phases of $NaErF_4$ and ZnO. The majority of α phase of $NaErF_4$ and hexagonal phased of ZnO were presented. Crystal surface (100), (002), (101), (102), (110) and (103) of samples were mainly attributed to the ZnO. Crystal surface (111), (200), (220), (311), and (400) of samples were corresponded to α-$NaErF_4$. These results indicated that $NaErF_4$ and ZnO upconversion nanoparticles compound was obtained.

To further reveal the successful preparation of $NaErF_4$@ZnO upconversion nanoparticles, transmission electron microscopy (TEM) images of $NaErF_4$ and $NaErF_4$@ZnO was showed in

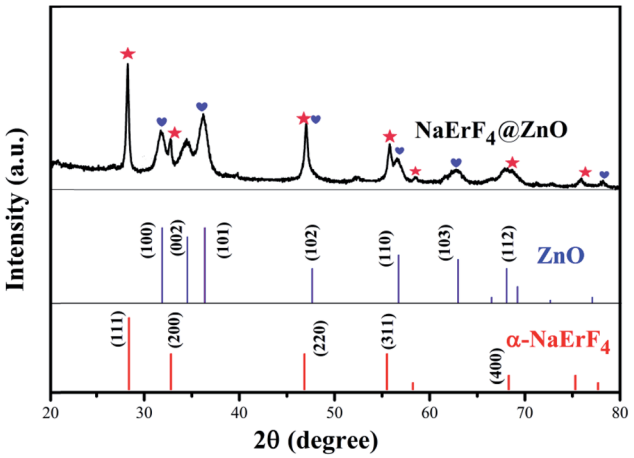

Fig. 2 X-ray diffraction patterns of $NaErF_4$@ZnO upconversion nanoparticles. The diffraction peaks of α-phase $NaErF_4$ and ZnO were marked by red and blue labels, respectively.

Fig. 3a and b. Without coating ZnO, the $NaErF_4$ was quadrilateral-like nanostructures, and the size of samples was about 17.1 nm. As illustrated in Fig. 3b and c, the size of nanoparticles increased to about 42 nm, and the quadrilateral-like nanostructure remained. High resolution TEM (HTEM) image (Fig. 3d) of a single nanoparticle taken from Fig. 3c presented the measured interplanar spacing of 0.28 nm and 0.31 nm, corresponding to the (100) crystal plane to hexagonal phase ZnO and the (111) crystal plane to α phase $NaErF_4$, respectively. Scanning Electron Microscopy (SEM) of $NaErF_4$@ZnO upconversion nanoparticles performed a tetrahedral structure in Fig. 3e. These results suggested that ZnO was coated on the $NaErF_4$ surface, forming $NaErF_4$@ZnO. In addition, energy dispersive X-ray spectrometer (EDS) mapping taken from Fig. 3e was analyzed in Fig. 3f. The EDS mapping showed the presence of Zn, O, Er and F elements, further confirming the

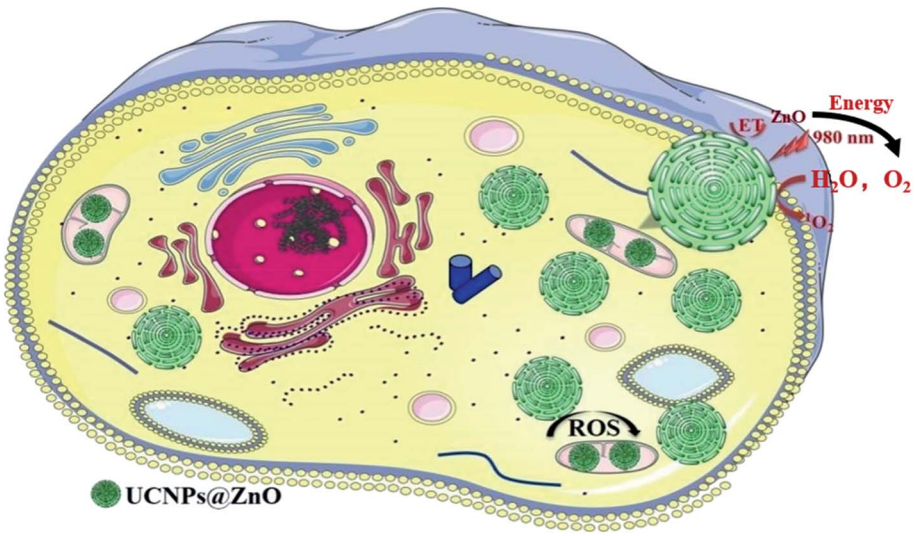

Fig. 1 Schematic illustration of photodynamic therapy mechanism of $NaErF_4$@ZnO upconversion nanoparticles in producing the ROS under the excitation at 980 nm. ET was the energy transfer process.

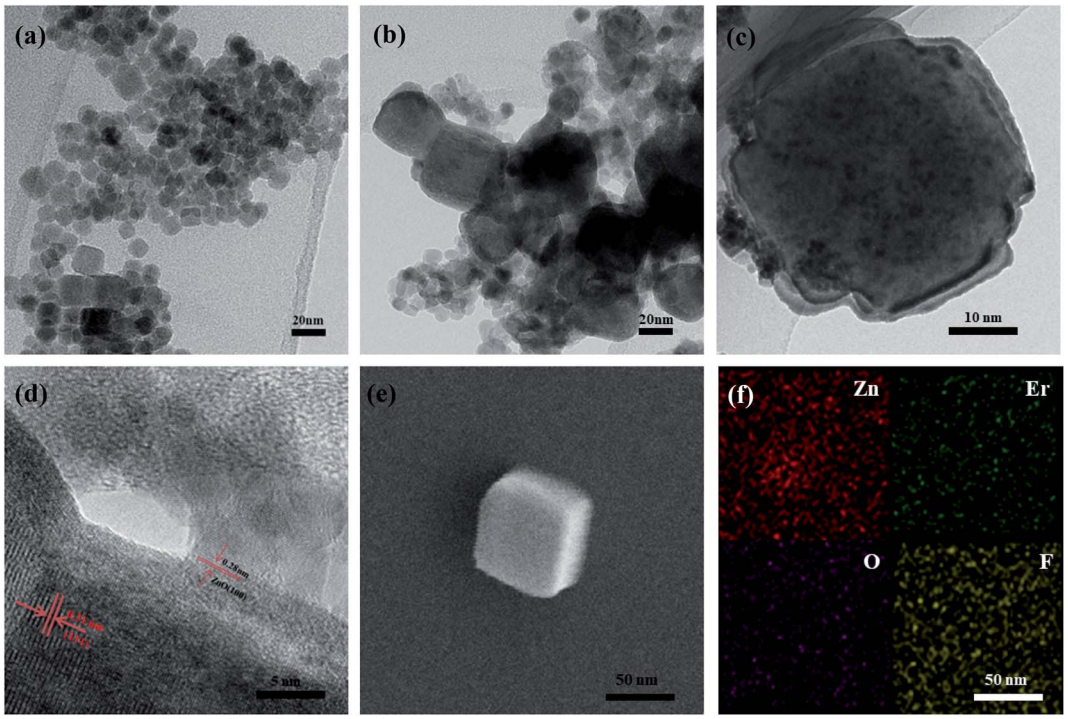

Fig. 3 (a) TEM image of $NaErF_4$ upconversion nanoparticles. (b) TEM image of $NaErF_4$@ZnO upconversion nanoparticles. (c) TEM image of $NaErF_4$@ZnO upconversion single particle. (d) HTEM image taken from single particle in (c) of $NaErF_4$@ZnO. (e) SEM image of $NaErF_4$@ZnO upconversion single particle. (f) EDS mapping of $NaErF_4$@ZnO upconversion nanoparticles. The brightness of the image represented the concentration of the element.

preparation of $NaErF_4$@ZnO upconversion nanoparticles. All these observations verified that ZnO was coated successfully on the $NaErF_4$ particles.

In order to investigate the luminescent properties of as-prepared $NaErF_4$@ZnO nanoparticles, the upconversion luminescent spectra of $NaErF_4$ and $NaErF_4$@ZnO was compared in Fig. 4a. It can be seen that the all upconversion emission intensity was increased by coating ZnO particles. While in $NaErF_4$@ZnO system, blue, green and red upconversion luminescence (UCL) of samples can be achieved and UCL intensities were enhanced by 27, 7 and 10 times compared to that of $NaErF_4$ (Fig. 4b), respectively. As demonstrated, upconversion spectrum showed emission bands centered at 525 nm (green UCL), 545 nm (green UCL) and 661 nm (red UCL), which can be assigned to the $^2H_{11/2} \rightarrow {}^4I_{15/2}$ transition, $^4S_{3/2} \rightarrow {}^4I_{15/2}$ transition and $^4F_{9/2} \rightarrow {}^4I_{15/2}$ transition of Er^{3+} ions (Fig. 4c), respectively. In addition, the UCL emission at 350∼400 nm was observed, which can excited the ZnO particle, sensitized reactive oxygen species generation from oxygen for photodynamic therapy (PDT). The blue UCL at 415 nm originated from $V_o^{2+} \rightarrow V_{Zn}$ energy level defect transition of ZnO, indicating ZnO was sensitized by UV light. This result confirmed that ZnO was coated on $NaErF_4$ in as-prepared upconversion nanoparticles. Since the production of singlet oxygen was based on 980 nm excitation NIR light, 980 nm NIR illumination improved the tissue penetration and enhanced the PDT efficiency. As performed in Fig. 4d, the ROS generation of $NaErF_4$@ZnO upconversion nanoparticles under 980 nm NIR light was measured *via* the absorbance of 1,3-diphenyliso-benzofuran (DPBF) at 488 nm. In Fig. 4d, the DPBF absorption intensity of $NaErF_4$@ZnO upconversion nanoparticles with 980 nm irradiation significantly decreased with increase time from 0 min to 30 min, suggesting that a more efficient ROS generation. In constant, the DPBF absorption intensity of only 980 nm irradiation or $NaErF_4$@ZnO nanoparticles had no obvious changing, indicating that only NIR light or materials cannot be produced ROS. This result can further verify that $NaErF_4$@ZnO upconversion nanoparticles can be sensitized to generate ROS under 980 nm excitation, which had great potential in the application of photodynamic therapy.

The $NaErF_4$@ZnO upconversion nanoparticles (UCNPs) had potential application in PDT due to their high ROS generation with NIR irradiation. Moreover, bio-toxicity had an important influence on the development of UCNPs for biological applications. In order to investigate the cytotoxicity of $NaErF_4$@ZnO upconversion nanoparticles (UCNPs) *in vitro*, the toxicity of $NaErF_4$@ZnO UCNPs without 980 nm NIR irradiation to cells was measured BHP 5-16 cells with CCK8 method. A CCK8 assay with BHP 5-16 cells was used to study the cytotoxicity of Yb/Tm/GZO@SiO_2 nanoparticles (Fig. 5a). BHP 5-16 cells viability can be followed eqn (1).[40]

$$\text{cell viability}(\%) = \frac{A_s - A_b}{A_c - A_b} \times 100\% \quad (1)$$

where A_s and A_b were the absorbance of test cells with $NaErF_4$@ZnO UCNPs and the absorbance of control cells

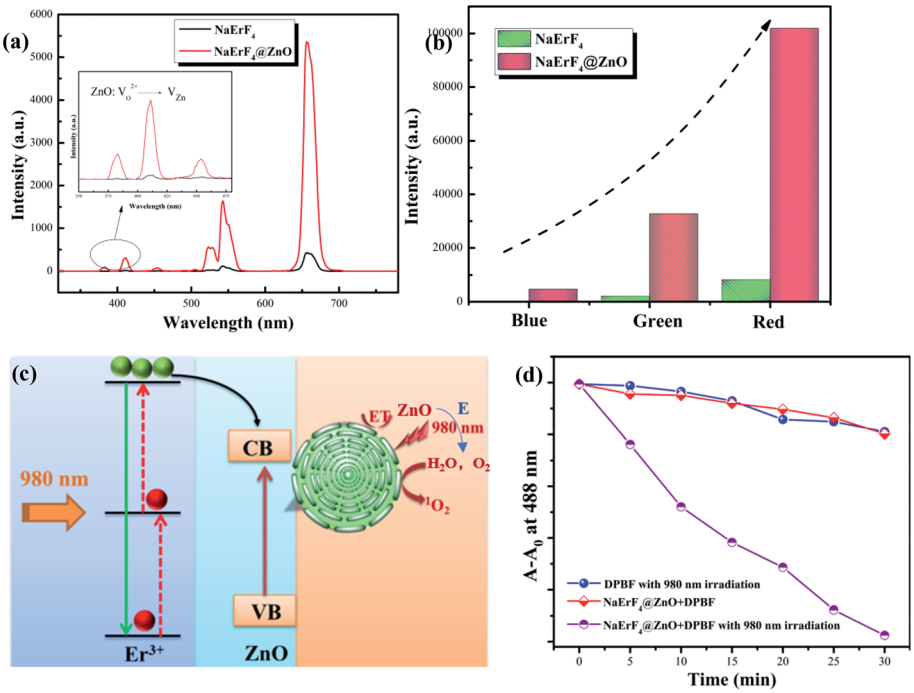

Fig. 4 (a) The upconversion luminescent spectra of $NaErF_4$ and $NaErF_4$@ZnO upconversion nanoparticles, the inset was the upconversion luminescent spectra range from 350 nm to 475 nm bands of samples. (b) The upconversion luminescent intensities of $NaErF_4$ and $NaErF_4$@ZnO nanoparticles. (c) Schematic illustration of upconversion energy transfer mechanism of $NaErF_4$@ZnO. ET was energy transfer and E was energy. (d) DPBF absorbance of $NaErF_4$@ZnO without 980 nm irradiation and 980 nm irradiation without $NaErF_4$@ZnO. DPBF absorbance of $NaErF_4$@ZnO with 980 nm irradiation with increasing of time. A and A_0 was DPBF absorption intensity and absorption intensity of control group, respectively.

without $NaErF_4$@ZnO UCNPs, respectively. A_c represented the absorbance of blank samples containing culture medium without cells and $NaErF_4$@ZnO UCNPs. As illustrated in Fig. 5a, the viability of cells was evaluated at three time points (12 h, 24 h and 48 h) after incubating with 400 μg mL^{-1}, 600 μg mL^{-1}, 800 μg mL^{-1} and 1000 μg mL^{-1} $NaErF_4$@ZnO UCNPs. Although the concentration of $NaErF_4$@ZnO UCNPs was as high as 1000 μg mL^{-1} for 48 h, the cell viabilities were greater than 94.88%, indicating the $NaErF_4$@ZnO UCNPs had a low toxicity to BHP 5-16 cells. These results demonstrated that $NaErF_4$@ZnO UCNPs had the low cytotoxicity, allowing for $NaErF_4$@ZnO UCNPs as PDT application. *In vitro* PDT therapeutic effects of $NaErF_4$@ZnO UCNPs were evaluated using the BHP 5-16 cells upon 980 nm NIR irradiation at different concentrations of UCNPs. BHP 5-16 cells were treated with UCNPs for 12h. BHP 5-16 cells were irradiated at a 980 nm laser with 0.6 W cm^{-2} for 30 min (the cell radiated at 2 min intervals), and the cell viability was determined with a CCK8 method. As shown in Fig. 5b, the cell

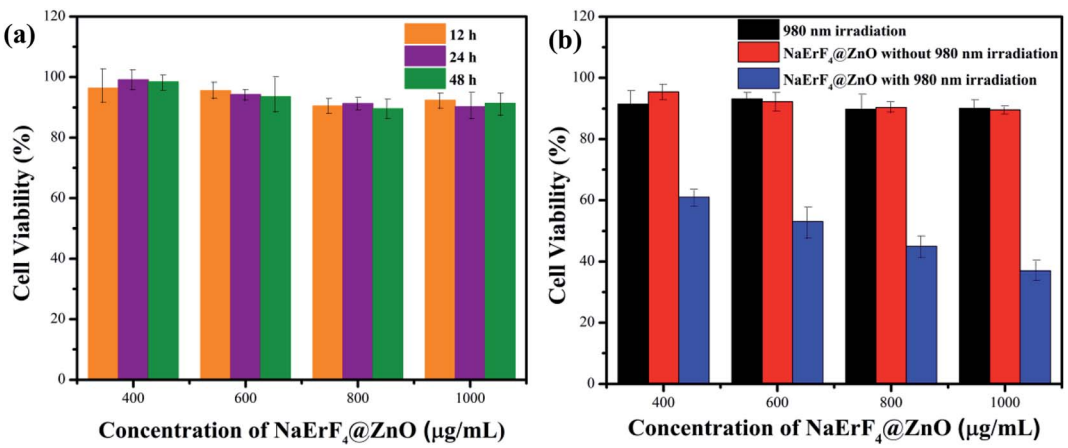

Fig. 5 (a) CCK8 assay of the BHP-5-16 cells viability after incubating with different changed $NaErF_4$@ZnO UCNPs concentrations ranging from 400 to 1000 μg mL^{-1} for 12 h, 24 h and 48 h. (each group $n = 4$) (b) CCK8 assay of $NaErF_4$@ZnO UCNPs with different concentrations with and without 980 nm NIR irradiation (0.6 W cm^{-2}, each group $n = 4$).

viabilities of only 980 nm irradiation without $NaErF_4$@ZnO UCNPs were about 91%, 96%, 89% and 90% at 400 μg mL^{-1}, 600 μg mL^{-1}, 800 μg mL^{-1} and 1000 μg mL^{-1} concentration of $NaErF_4$@ZnO UCNPs, respectively. It can be seen that 980 nm irradiation without $NaErF_4$@ZnO UCNPs had no significant impact on cell growth. The cell viabilities of only $NaErF_4$@ZnO UCNPs without 980 nm irradiation were about 98%, 95%, 92% and 89% at 400 μg mL^{-1}, 600 μg mL^{-1}, 800 μg mL^{-1} and 1000 μg mL^{-1} concentration of $NaErF_4$@ZnO UCNPs, respectively. This result confirmed the cell viability did not change too much for $NaErF_4$@ZnO UCNPs, despite the existence of a high concentration of 1000 μg mL^{-1}. Apparently, the cell viabilities were about 60%, 57%, 44% and 41% at increase concentration of $NaErF_4$@ZnO UCNPs from 400 μg mL^{-1} to 1000 μg mL^{-1} with NIR 980 nm laser irradiation. With increasing of concentration of $NaErF_4$@ZnO UCNPs, BHP 5-16 cells viability gradually decreased under 980 nm excitation. It was worth noting that only $NaErF_4$@ZnO UCNPs with 980 nm irradiation simultaneous existed, the cell survival rate can be significantly decreased, which further verified that $NaErF_4$@ZnO UCNPs can generated ROS with 980 nm laser irradiation. This indicated that $NaErF_4$@ZnO UCNPs had a good PDT effect on BHP 5-16 cells.

To further explore the PDT effect of $NaErF_4$@ZnO UCNPs in BHP 5-16 cells *in vitro*, the production of ROS was measured though DCFH-DA probe. If there was ROS, it would show obvious fluorescence green images by DCFH-DA probe. Fig. 6a performed that control group had no markedly green light image, indicating without ROS expression. As shown in Fig. 6b and c, the images had no green fluorescence and cell morphology was intact structure at the 980 nm irradiation without $NaErF_4$@ZnO UCNPs group and $NaErF_4$@ZnO UCNPs without 980 nm irradiation at concentration of 800 μg mL^{-1}. These results indicated that $NaErF_4$@ZnO UCNPs and 980 nm irradiation had no damage the cell and had no produce ROS. When concentration of $NaErF_4$@ZnO was 400 μg mL^{-1} with 980 nm irradiation, the image presented green light expression and BHP 5-16 cells had some damage (Fig. 6d). This suggested that ROS produced at 400 μg mL^{-1} of $NaErF_4$@ZnO with 980 nm irradiation. The brightness of green light enhanced and most of cells had died with increase $NaErF_4$@ZnO concentration from 600 μg mL^{-1} to 800 μg mL^{-1} with 980 nm irradiation (Fig. 6e and f), which consistent with ROS level of $NaErF_4$@ZnO UCNPs increasing with rising of concentrations. It was further indicated that $NaErF_4$@ZnO UCNPs had an excellent application in photodynamic therapy.

Conclusion

In summary, a novel $NaErF_4$@ZnO UCNPs was synthesized. The UCL emission of $NaErF_4$ was used to sensitize ZnO. The ZnO as a photosensitizer can produce the ROS. The unique combination of $NaErF_4$ and ZnO UCNPs can be used for PDT of thyroid cancer cell. ROS generation of $NaErF_4$@ZnO upconversion nanoparticles with 980 nm NIR light was measured *via* the absorbance of DPBF, suggesting sensitization of ROS production with $NaErF_4$@ZnO. Meanwhile, the toxicity of BHP 5-16 cells was evaluated by CCK8 assay. The viability of BHP 5-16 cells has no damage at 1000 μg mL^{-1} of $NaErF_4$@ZnO for 48 h, indicating this nanoparticle had low toxic for BHP 5-16 cells. The results of CCK8 assay performed that 60%∼41% cell viability can be obtained for $NaErF_4$@ZnO UCNPs at the

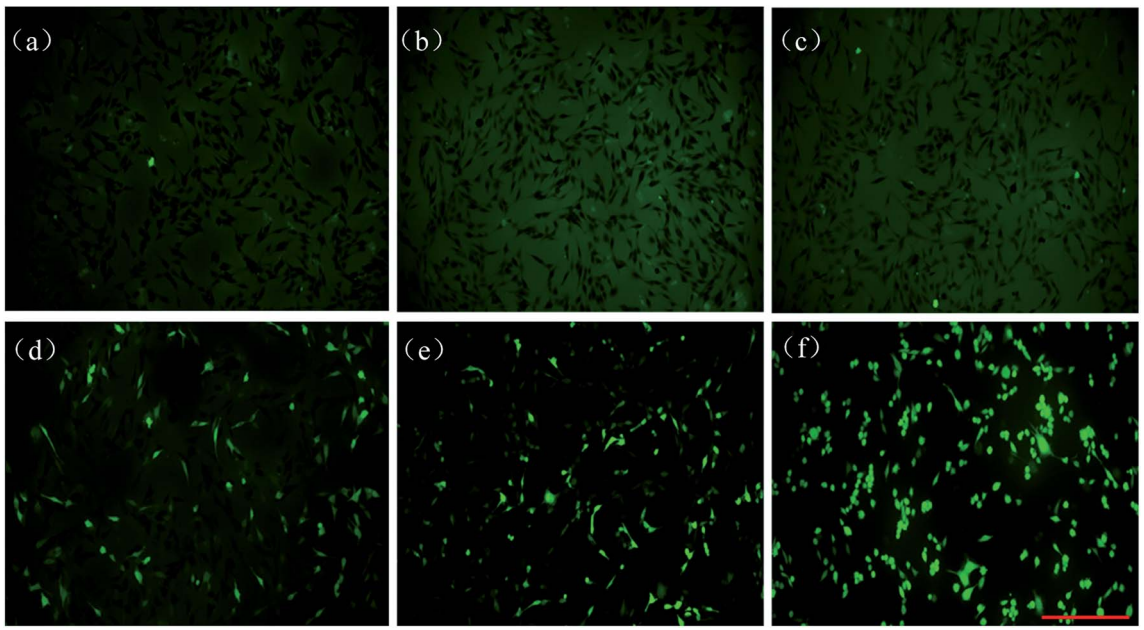

Fig. 6 The production of ROS measured by DCFH-DA probe. (Image scale in a–f: 400 μm) (a) BHP 5-16 cells image of control group, (b) the 980 nm irradiation without $NaErF_4$@ZnO UCNPs group, (c) $NaErF_4$@ZnO UCNPs without 980 nm irradiation group at concentration of 800 μg mL^{-1}, (d) $NaErF_4$@ZnO UCNPs with 980 nm irradiation group at concentration of 400 μg mL^{-1}, (e) $NaErF_4$@ZnO UCNPs with 980 nm irradiation group at concentration of 600 μg mL^{-1} and (f) $NaErF_4$@ZnO UCNPs with 980 nm irradiation group at concentration of 800 μg mL^{-1}.

concentration from 400 μg mL^{-1} to 1000 μg mL^{-1} with 30 min 980 nm NIR irradiation. The image based on dihydroethidium staining presented the highest green light with 800 μg mL^{-1} of $NaErF_4$@ZnO compared with that of 400 μg mL^{-1} and 600 μg mL^{-1}, which consistent with the dosage concentrations required for PDT of papillary thyroid cancer.

Experiment

Synthesis of $NaErF_4$ core upconversion nanoparticles

The NaOH of 0.6 g was dissolved in 5 mL deionized water, and added oleic acid (10 mL) with ultrasound for 20 min. $Er(NO_3)_3 \cdot 5H_2O$ (1 mmol), $Yb(NO_3)_3 \cdot 5H_2O$ (20 mol%) and NaF (8 mmol) were dissolved while stirring for 2 h at 25 °C. After this procedure, the resulting solution was transferred to the reaction kettle (30 mL) and reacted at 140 °C for 12 h. The obtained $NaErF_4$ sample was cooled down to room temperature, and cleaned by centrifugation with deionized water and ethanol. The core upconversion nanoparticles were achieved.

Synthesis of $NaErF_4$@ZnO upconversion nanoparticles

As-synthesized $NaErF_4$ nanoparticles was dispersed in 30 mL ethanol and 20 mL deionized water with ultrasonic for 30 min of water and solution and ultrasonic wave for 30 min. CTAB (0.3 mmol) was added into this suspension with ultrasonic for 10 min. And then ascorbic acid (0.2 mmol), hexamethylenetetramine (1 mmol) and $Zn(NO_3)_2 \cdot 6H_2O$ (1 mmol) were added into the previous mixture with magnetic stirring for 1 h in room temperature, and heated up to 85 °C for 10 h. The samples were cleaned by centrifugation with deionized water and ethanol, and dried in an oven for 24 h. The obtained samples were annealed for 2 h at 350 °C in the muffle furnace. The $NaErF_4$@ZnO core/shell upconversion nanoparticles (UCNPs) was obtained.

Characterization of the $NaErF_4$@ZnO (UCNPs)

TEM images was obtained with JEM-2100. Elemental analysis was achieved with an energy-dispersive X-ray (EDX) by TEM. The X-ray diffraction (XRD) of the $NaErF_4$ and $NaErF_4$@ZnO was collected by a diffractometer with Cu Kα that worked at 40.0 kV and 30.0 mA. The upconversion fluorescence spectrometer was measured with 980 nm laser excitation.

Cell culture

The BHP 5-16 cells were cultured RPMI 1640 (Hyclone, China) supplemented with 10% fetal bovine serum (Gibico, USA) and 1% penicillin–streptomycin (Solarbio, China). Cells were maintained in a humidified incubator (Thermo Forma, USA) containing 5% CO_2 at 37 °C, and all the experiments were performed in a clean atmosphere.

In vitro cytotoxicity evaluation

A Cell Counting Kit-8 (CCK-8) (Beyotime Institute of Biotechnology) was used for the evaluation of cell cytotoxicity. A total of 5000 cells were seeded into 96 well plates, which were cultured in AIM medium and treated with different concentrations of NaErF4@ZnO UCNPs (400 μg mL^{-1}, 600 μg mL^{-1}, 800 μg mL^{-1}, 1000 μg mL^{-1}) in a humidified atmosphere at 37 °C with 5% CO_2 for 12 h, 24 h and 48 h, respectively. CCK-8 (10 μL) was added into each well and incubated for 1.5 h at 37 °C. The absorbance was measured using the iMark Microplate Reader at a wavelength of 450 nm (BIO-RAD Instruments, USA).

In vitro ROS generation assay

The Reactive Oxygen Species Assay Kit (Beyotime Institute of Biotechnology) was used for the detection of intracellular ROS. BHP 5-16 (2×10^7) cells were seeded into 24 well plates, which were cultured in 1640 medium and treated with different concentrations of $NaErF_4$@ZnO UCNPs (400 μg mL^{-1}, 600 μg mL^{-1}, 800 μg mL^{-1}). The medium was discarded and added fresh 1640 medium after 12 h, then the samples were irradiated at a 980 nm laser with 0.6 W cm^{-2} for 30 min, 500 μL DCFH-DA reagent was added into each well and incubated for 20 min at 37 °C. The fluorescence images were achieved with a fluorescence microscope at a wavelength of 488 nm.

Conflicts of interest

There are no conflicts to declare.

Acknowledgements

This work was financially supported by the Science & Technology Development Fund of Tianjin Education Commission for Higher Education (No. 2018KJ069) and Startup Funding of Scientific Research, Tianjin Medical University Metabolic Diseases Hospital and Tianjin Institute of Endocrinology (No. 2017DX07).

References

1 C. A. Robertson, D. H. Evans and H. Abrahamse, Photodynamic therapy (PDT): a short review on cellular mechanisms and cancer research applications for PDT, *J. Photochem. Photobiol., B*, 2009, **96**, 1–8.
2 J. Jin, Y. Zhu, Z. Zhang and W. Zhang, Enhancing the efficacy of photodynamic therapy (PDT) through a porphyrin/POSS alternating copolymer, *Angew. Chem.*, 2018, **57**, 16354–16358.
3 K. Wang, Z. Zhang, L. Lin, J. Chen, K. Hao, H. Tian and X. Chen, Covalent organic nanosheets integrated heterojunction with two strategies to overcome hypoxic-tumor photodynamic therapy, *Chem. Mater.*, 2019, **31**, 3313–3323.
4 P. Ray, B. W. Huang and Y. Tsuji, Reactive oxygen species (ROS) homeostasis and redox regulation in cellular signaling, *Cell. Signalling*, 2012, **24**, 981–990.
5 R. D. Guzy, M. M. Mack and P. T. Schumacker, Mitochondrial complex III is required for hypoxia-induced ROS production and gene transcription in yeast, *Antioxid. Redox Signaling*, 2007, **9**, 1317–1328.

6 K. K. Griendling and G. FitzGerald, Oxidative stress and cardiovascular injury part I: basic mechanisms and *in vivo* monitoring of ROS, *Circulation*, 2003, **108**, 1912–1916.

7 J. C. Kennedy, R. H. Pottier and D. C. Pross, Photodynamic therapy with endogenous protoporphyrin IX: basic principles and present clinical experience, *J. Photochem. Photobiol., B*, 1990, **6**, 143–148.

8 R. Bonnett, Photosensitizers of the porphyrin and phthalocyanine series for photodynamic therapy, *Cheminform*, 1995, **26**, 19–33.

9 D. Kessel, Y. Luo, Y. Deng and C. K. Chang, The role of subcellular localization in initiation of apoptosis by photodynamic therapy, *Photochem. Photobiol.*, 2010, **65**, 422–426.

10 D. Bechet, P. Couleaud, F. Céline, M. Viriot, F. Guillemin and M. Barberi, Nanoparticles as vehicles for delivery of photodynamic therapy agents, *Trends Biotechnol.*, 2008, **26**, 612–621.

11 S. M. Halpern, A. V. Anstey, R. S. Dawe, B. L. Diffey, P. M. Farr, J. Ferguson, J. L. Hawk, S. Ibbotson, J. M. McGregor, G. M. Murphy, S. E. Thomas and L. E. Rhodes, Guidelines for topical photodynamic therapy: report of a workshop of the British photodermatology group, *Br. J. Dermatol.*, 2015, **142**, 22–31.

12 A. P. Castano, P. Mroz and M. R. Hamblin, Photodynamic therapy and anti-tumour immunity, *Nat. Rev. Cancer*, 2006, **6**, 535–545.

13 C. Chen, X. Ni, S. Jia, Y. Liang, X. Wu, D. Kong and D. Ding, Massively evoking immunogenic cell death by focused mitochondrial oxidative stress using an AIE luminogen with a twisted molecular structure, *Adv. Mater.*, 2019, **31**, 1904914.

14 X. Ni, X. Zhang, X. Duan, H. Zheng, X. Xue and D. Ding, Near-Infrared afterglow luminescent aggregation-induced emission dots with ultrahigh tumor-to-liver signal ratio for promoted image-guided cancer surgery, *Nano Lett.*, 2019, **19**, 318–330.

15 C. Chen, H. Ou, R. Liu and D. Ding, Regulating the photophysical property of organic/polymer optical agents for promoted cancer phototheranostics, *Adv. Mater.*, 2020, **32**, 1806331.

16 C. Chen, X. Ni, H.-W. Tian, Q. Liu, D.-S. Guo and D. Ding, Calixarene-based supramolecular AIE dots with highly inhibited nonradiative decay and intersystem crossing for ultrasensitive fluorescence image-guided cancer surgery, *Angew. Chem., Int. Ed.*, 2020, **59**, 10008.

17 H. Fang, S. Xu and B. Liu, Photosensitizers with aggregation-induced emission: materials and biomedical applications, *Adv. Mater.*, 2018, **30**, e1801350.

18 R. R. Allison, G. H. Downie, R. Cuenca, X. Hu, J. Carter and C. Sibata, Photosensitizers in clinical PDT, *Photodiagn. Photodyn. Ther.*, 2004, **1**, 27–42.

19 J. Berlanda, T. Kiesslich, V. Engelhardt, B. Krammer and K. Plaetzer, Comparative *in vitro* study on the characteristics of different photosensitizers employed in PDT, *J. Photochem. Photobiol., B*, 2010, **99**, 173–180.

20 G. Chen, H. Qiu, P. N. Prasad and X. Chen, Upconversion nanoparticles: design, nanochemistry, and applications in theranostics, *Chem. Rev.*, 2014, **114**, 5161–5214.

21 C. Wang, H. Tao, L. Cheng and Z. Liu, Near-infrared light induced *in vivo* photodynamic therapy of cancer based on upconversion nanoparticles, *Biomaterials*, 2011, **32**, 6145–6154.

22 F. Wang, J. Wang and X. Liu, Direct evidence of a surface quenching effect on size-dependent luminescence of upconversion nanoparticles, *Angew. Chem.*, 2010, **122**, 7618–7622.

23 L. Xiong, Z. Chen, Q. Tian, T. Cao, C. Xu and F. Li, High contrast upconversion luminescence targeted imaging *in vivo* using peptide-labeled nanophosphors, *Anal. Chem.*, 2009, **81**, 8687–8694.

24 J. Silver, M. I. Martinez-Rubio, T. G. Ireland, R. George and R. Withnall, Effect of particle morphology and crystallite size on the upconversion luminescence properties of erbium and ytterbium co-doped yttrium oxide phosphors, *Cheminform*, 2001, **32**, 948–953.

25 F. Zhang, Y. Wan, T. Yu, F. Zhang, Y. Shi, S. Xie, Y. Li, L. Xu, B. Tu and D. Zhao, Uniform nanostructured arrays of sodium rare-earth fluorides for highly efficient multicolor upconversion luminescence, *Angew. Chem.*, 2007, **119**, 8122–8125.

26 H. Song, B. Sun, T. Wang, S. Lu, L. Yang, B. Chen, X. Wang and X. Kong, Three-photon upconversion luminescence phenomenon for the green levels in Er^{3+}/Yb^{3+} codoped cubic nanocrystalline yttria, *Solid State Commun.*, 2004, **132**, 409–413.

27 J. Wang, R. Li, Z. Zhang, W. Sun, R. Xu, Y. Xie, Z. Xing and X. Zhang, Efficient photocatalytic degradation of organic dyes over titanium dioxide coating upconversion luminescence agent under visible and sunlight irradiation, *Appl. Catal., A*, 2008, **334**, 227–233.

28 I. P. Yong, H. N. Sang and J. H. Kim, Comparative Study of Upconverting Nanoparticles with Various Crystal Structures, Core/Shell Structures, and Surface Characteristics, *J. Phys. Chem. C*, 2013, **117**, 2239–2244.

29 Z. Yi, X. Li, Z. Xue, X. Liang, W. Lu, H. Peng, H. Liu, S. Zeng and J. Hao, Tumor detection: Remarkable NIR enhancement of multifunctional nanoprobes for *in vivo* trimodal bioimaging and upconversion optical/T2-weighted MRI-guided small tumor diagnosis, *Adv. Funct. Mater.*, 2015, **25**, 7102.

30 Z. Xue, Z. Yi, X. Li, Y. Li, M. Jiang, H. Liu and S. Zeng, Upconversion optical/magnetic resonance imaging-guided small tumor detection and *in vivo* tri-modal bioimaging based on high-performance luminescent nanorods, *Biomaterials*, 2017, **115**, 90–103.

31 D. Song, S. Chi, X. Li, C. Wang, Z. Li and Z. Liu, Upconversion system with quantum dots as sensitizer: Improved photoluminescence and PDT efficiency, *ACS Appl. Mater. Interfaces*, 2019, **11**, 41100–41108.

32 C. Wang, L. Cheng and Z. Liu, Upconversion nanoparticles for photodynamic therapy and other cancer therapeutics, *Theranostics*, 2013, **3**, 317–330.

33 Q. Q. Dou, A. Rengaramchandran, S. T. Selvan, R. Paulmurugan and Y. Zhang, Core–shell upconversion nanoparticle-semiconductor heterostructures for photodynamic therapy, *Sci. Rep.*, 2015, **5**, 8252.

34 H. J. Wang, R. Shrestha and Y. Zhang, Encapsulation of photosensitizers and upconversion nanocrystals in lipid micelles for photodynamic therapy, *Part. Part. Syst. Charact.*, 2013, **31**, 228–235.

35 D. Bechet, P. Couleaud, F. Céline, M. Viriot and F. Guillemin, Nanoparticles as vehicles for delivery of photodynamic therapy agents, *Trends Biotechnol.*, 2008, **26**, 612–621.

36 S. P. Singh, Multifunctional magnetic quantum dots for cancer theranostics, *J. Biomed. Nanotechnol.*, 2011, **7**, 95–97.

37 W. Chen, Nanoparticle self-lighting photodynamic therapy for cancer treatment, *J. Biomed. Nanotechnol.*, 2008, **4**, 369–376.

38 X. Wang, X. Kong, Y. Yu, Y. Sun and H. Zhang, Effect of annealing on upconversion luminescence of ZnO:Er^{3+} nanocrystals and high thermal sensitivity, *J. Phys. Chem. C*, 2007, **111**, 15119–15124.

39 Y. Sun, Y. Chen, L. Tian, Y. Yu, X. Kong, Q. Zeng, Y. Zhang and H. Zhang, Morphology-dependent upconversion luminescence of ZnO:Er^{3+} nanocrystals, *J. Lumin.*, 2008, **128**, 15–21.

40 Y. Li, R. Wang, Y. Xu, W. Zheng and Y. M. Li, Influence of silica surface coating on operated photodynamic therapy property of Yb^{3+}–Tm^{3+}: Ga(III)-doped ZnO upconversion nanoparticles, *Inorg. Chem.*, 2018, **57**, 8012–8018.